

Damping rates of hard momentum particles in a cold ultrarelativistic plasma

Benoît Vanderheyden

Department of Physics, University of Illinois at Urbana-Champaign, Urbana, IL 61801

Jean-Yves Ollitrault*

Service de Physique Théorique[†], CE-Saclay, 91191 Gif-sur-Yvette cedex, France

(July 14, 2018)

Abstract

We compute the damping rates of one-particle excitations in a cold ultrarelativistic plasma to leading order in the coupling constant e for three types of interaction: Yukawa coupling to a massless scalar boson, QED and QCD. Damping rates of charged particles in QED and QCD are of order $e^3\mu$, while damping rates of other particles are of order $e^4\mu$ or $e^4\mu \log(1/e)$. We find that the damping rate of an electron or of a quark is constant far from the Fermi surface, and decreases linearly with the excitation energy close to the Fermi surface. This unusual behavior is attributed to the long-range magnetic interactions.

*Affiliated with CNRS

[†]Laboratoire de la Direction des Sciences de la Matière du Commissariat à l'Énergie Atomique

I. INTRODUCTION

The quasiparticle concept is a powerful tool for studying the dynamical properties of ultrarelativistic plasmas; it has been widely used in the recent literature [1]. Weakly excited states of a plasma can be described as superpositions of quasiparticle states, which behave, at least in a first approximation, as free, non-interacting, particles. These elementary excitations undergo damping through their mutual coupling, which gives their energy spectrum a finite width. The quasiparticle concept holds only if this energy spread, or equivalently the damping rate, is negligible compared to the mean energy of their wave packet.

In this paper, we compute damping rates in plasmas at high density and zero temperature, $T = 0$. While the thermodynamic properties of ultrarelativistic degenerate plasmas are well known [2], little work has been devoted so far to their dynamical properties [3,4]. Most works on damping rates have been focusing on plasmas at high temperature with vanishing chemical potential, $\mu = 0$. However, plasmas with finite chemical potential are also relevant in view of phenomenological applications: first, degenerate quark systems (with $\mu \ll T$) might exist in the cores of neutron stars [5]; second, the state of the hadronic matter (possibly a quark-gluon plasma) temporarily formed in an ultrarelativistic nucleus-nucleus collision corresponds to values of μ and T of the same order of magnitude at the presently available energies [6].

From a theoretical point of view, the zero temperature case owes its interest to the basic difference, compared to the high temperature limit, in the infrared divergences which plague perturbative calculations in gauge theories. Naive perturbation theory leads to two levels of infrared divergences [7,8]. Those appearing in the calculation of transport coefficients [9] and collisional energy loss [10] are cured by taking into account screening effects at the one-loop level: propagators and vertices must be corrected at long wavelengths, according to the resummation scheme developed by Braaten and Pisarski [11]. The momentum and energy dependence of these medium effects is the same for hot ($\mu = 0$) and cold ($T = 0$) relativistic plasmas, and is characterized by a scale of order eT for a hot plasma, and $e\mu$ for

a cold plasma. At high temperature, the lack of static screening of the transverse part of the interaction is responsible for a logarithmic divergence in the perturbative calculation of the fermion damping rate [12–14]. This problem has been recently solved in hot QED [15]. By contrast, this second level of divergence does not appear at zero temperature, because of Pauli blocking. This allows us to obtain finite, most often analytical expressions for the damping rates $\Gamma(p)$ of all one-particle excitations, as a function of their momentum p .

Three types of interactions are discussed and compared. (1) Electromagnetic interaction (QED): this corresponds to a degenerate electron gas. (2) Non-abelian $SU(N_c)$ interaction (QCD): for $N_c = 3$, this corresponds to degenerate quark matter. (3) In addition, we consider a toy model where the fermion field $\psi(x)$ is coupled to a massless scalar field $\phi(x)$, with the Yukawa interaction $\mathcal{L}_Y = e\bar{\psi}\psi\phi$. These theories share several features. The resummed fermion propagator is the same for the three theories. The resummed boson propagator is the same for the two gauge theories, QED and QCD, while screening corrections reduce to a medium-induced mass term [16] for the Yukawa interaction. The coupling constant, noted e for all theories, will be assumed to be much smaller than unity, $e \ll 1$, to ensure that a perturbative expansion is reliable. It has been shown that perturbation theory can be used to study the properties of the QCD phase if the temperature and/or the chemical potential is much larger than Λ_{QCD} [2].

We are considering degenerate Fermi systems in their ground state. Single particle excitations are obtained by adding or removing one particle from the ground state, and damping of these excitations results from collisions with the fermions of the Fermi sea. Two types of excitations compose the quasiparticle spectrum. At large (“hard”) momenta p , $p \sim \mu \gg e\mu$, the elementary modes correspond to single particles slightly perturbed by the medium. Their damping processes are the object of this paper. For hard fermion or hole excitations, the only collisional process to leading order in e is elastic (Møller) scattering $ff \rightarrow ff$. [We use the generic names bosons (b), fermions (f) and antifermions (\bar{f}).] For an antifermion, two processes may contribute, namely elastic (Bhabha) scattering $\bar{f}f \rightarrow \bar{f}f$ and pair annihilation $\bar{f}f \rightarrow bb$. For a boson, the only process is elastic (Compton) scattering

$bf \rightarrow bf$. On the other hand, long wavelength (“soft”) modes, of momentum p of order $e\mu$, correspond to collective oscillations in the medium. Their damping processes are more complex: to leading order in e , bremsstrahlung contributes: $ff \rightarrow ffb$ for a soft hole, or $\bar{f}ff \rightarrow bf$ for a soft antifermion. A discussion of these calculations will be presented in a forthcoming publication [17].

Depending on the interaction and on the type of excitation considered, the dominant contribution to the damping rate may come either from processes with large scattering angles ($\theta \sim 1$), from processes with small scattering angles ($\theta \sim e$), or from both. Large scattering angles correspond to hard exchanged quanta, for which medium effects are small: then, the amplitudes are the same as in the vacuum. On the other hand, if a hard particle of momentum $p \sim \mu$ is deflected by an angle of order e , the exchanged quantum has a soft momentum of order $e\mu$, for which medium effects become important. In section II, we estimate the orders of magnitude of both hard and soft contributions to the damping rates. We show how they can be calculated, in a kinetic approach, as phase space integrals of elementary scattering processes. The equivalence with field theoretical methods is recalled in Appendix B. Section III presents the calculations of damping rates for the various excitations considered, while section IV is devoted to a discussion of the results along with a comparison between damping rates in cold and hot plasmas.

II. GENERAL ANALYSIS

A. Orders of magnitude

The damping rate Γ , the number of collisions per unit time, is of order $\Gamma \sim \sigma n v$ where σ is the scattering cross section, n the density of scatterers and v the relative velocity. In this paper, we assume that all particles are massless, which implies $v = 1$ ($\hbar = c = 1$). We consider $2 \rightarrow 2$ elementary processes in which an incoming particle of four-momentum $P = (p, \mathbf{p})$ (fermion above the Fermi level, antifermion or boson) is added to the system

and scatters on a particle of the Fermi sea with four-momentum $K = (k, \mathbf{k})$, $k < \mu$. We denote by $P' = (p', \mathbf{p}')$ and $K' = (k', \mathbf{k}')$ the four-momenta of outgoing particles. If the excitation under study is a hole in the Fermi sea, incoming and outgoing particles must be interchanged. The differential cross section for unpolarized particles can generally be written as

$$\frac{d\sigma}{dt} = \frac{1}{32\pi s^2} \overline{|M|^2}, \quad (1)$$

where $\overline{|M|^2}$ denotes the scattering matrix element squared, averaged over the helicity states of the incoming particle with momentum \mathbf{p} , and summed over the helicity states of the other particles. (Note that we do a sum, rather than an average, over the 2 helicity states of the scatterer. This unusual convention will turn out to be convenient in the following sections.) A factor 1/2 is included in $\overline{|M|^2}$ if the outgoing particles are identical. The variables $s = (P + K)^2$, $t = (P - P')^2$ and $u = (P - K')^2 = -s - t$ are the usual Mandelstam variables. In the center of mass frame, t is related to the momentum transfer q by $t = -q^2$ and to the scattering angle θ by $t = -s \sin^2(\theta/2)$. In order to obtain the total cross section, one must integrate eq. (1) over t between $t = -s$ and $t = 0$.

For a given scattering process in the plasma, the squared matrix element $\overline{|M|^2}$ is deduced from the usual Feynman rules with appropriate corrections taking into account medium polarization effects. We distinguish three cases, depending on the behaviour of $\overline{|M|^2}$ at small t :

1) The tree matrix element $\overline{|M|^2}$ is finite at small momentum transfers: one example is fermion-fermion scattering in a Yukawa theory, for which the tree matrix element is

$$\overline{|M|^2} = 3e^4. \quad (2)$$

The total cross section is therefore finite and of order $\sigma \sim e^4/\mu^2$, since s is of order μ^2 . The density of particles per unit volume in the Fermi sea is of order $n \sim \mu^3$, which gives $\Gamma \sim e^4\mu$.

2) $\overline{|M|^2}$ is proportional to $1/t^2$ at small t : the differential cross section grows like $1/\theta^4$ at small scattering angle θ , which makes the total cross section diverge. This occurs in collisions

between charged particles (Rutherford divergence). For electron–electron scattering in QED (Møller scattering),

$$\overline{|M|^2} = 4e^4 \left(\frac{u}{t} + \frac{t}{u} + 1 \right)^2, \quad (3)$$

so that the total cross section diverges linearly in the infrared: $d\sigma \sim e^4 dt/t^2$. However, in a plasma, due to the screening of the electric charge, the interaction potential decreases exponentially for distances larger than the Debye screening length $r_D \sim 1/(e\mu)$. This causes a saturation of the differential cross section for momentum transfers $q < r_D^{-1} \sim e\mu$, i.e. for scattering angles $\theta < e$, or equivalently for $t < t_{\min} = e^2\mu^2$. The total cross section is therefore of order $\sigma \sim e^4/t_{\min} \sim e^2/\mu^2$. Note that this argument is not completely valid for the transverse part of the interaction, which is screened dynamically only (i.e. at finite energy transfer). However, as we shall show in detail later, dynamical screening is sufficient at zero temperature to saturate the damping rate at small momentum transfer. Now, for small momentum transfers of order $e\mu$, the density of scatterers is no longer $n \sim \mu^3$: because of Pauli blocking, the outgoing electron must have an energy larger than the Fermi energy μ , and only the electrons just below the Fermi surface can contribute, within an interval of order $e\mu$. Their density is $n \sim e\mu^3$, and one finally obtains $\Gamma \sim \sigma n \sim e^3\mu$.

3) $\overline{|M|^2}$ is proportional to $1/t$ at small t . This happens in processes where the exchanged particle is a massless fermion, such as pair annihilation and Compton scattering. For instance, in the Yukawa theory, the square tree matrix element for pair annihilation into two massless Yukawa bosons ($f\bar{f} \rightarrow bb$) is

$$\overline{|M|^2} = \frac{e^4}{2} \left(\frac{u}{t} + \frac{t}{u} - 2 \right), \quad (4)$$

and the total cross section diverges logarithmically in the infrared, rather than linearly in the previous case. This divergence is also cured by collective effects, which become important when the momentum transfer is of order $e\mu$. Note that these medium effects are taken into account in the fermion propagator, instead of the boson propagator in the previous case. Following the same reasoning, the total cross section is thus of order $\sigma = e^4 \ln(1/e)/\mu^2$.

For an annihilation process, there is no Pauli blocking in the final state, and the density of scatterers is of order $n \sim \mu^3$, hence the damping rate is of order $\Gamma \sim e^4 \ln(1/e)\mu$. In the case of Compton scattering, this last remark applies only for a boson whose energy is larger than the Fermi energy, so that it can turn into a fermion with almost the same momentum. Otherwise, Pauli blocking alone inhibits the infrared divergence and the damping rate is of order $e^4\mu$ (section III D).

These considerations on orders of magnitude allow us to simplify the damping rate calculation. In case 1), kinematics is dominated by hard momentum transfer (the “hard sector contribution”): the phase space for soft momentum transfer (the “soft sector contribution”) is smaller by a factor e . On the other hand, soft momentum transfer dominates in case 2); the differential cross section integrated over momentum transfer of order $e\mu$ is larger by a factor $1/e^2$ than the contribution from hard momentum transfer, while the phase space is smaller by only a factor e . Finally, in case 3), both hard and soft sector contributions are of equal magnitude.

We separate the hard and soft scales by introducing an arbitrary IR (resp. UV) momentum cutoff q_* in the hard (resp. soft) contribution. The cutoff q_* is chosen at an intermediate scale, $e\mu \ll q_* \ll \mu$. The hard and soft sector contributions to the damping rate are both computed in the framework of kinetic theory. For $q > q_*$ (hard contribution), collective effects are negligible since $q \gg e\mu$, and the damping rate can be calculated from the vacuum scattering amplitudes, integrated over phase space with an appropriate choice of variables, described in section II B. For $q < q_*$ (soft contribution), medium effects must be taken into account, but the kinematics is simplified by the fact that the exchanged particle is much softer than the external ones. The damping rate is most simply calculated as the emission probability of a soft, off-shell quantum, as developed in section II C. In case 3), both approximations are compatible in the region of the cutoff, so that the total damping rate, which is the sum of the two contributions, does not depend on the cutoff q_* [18].

Note that processes involving soft external particles, either incoming or outgoing, are subleading because the associated phase space is small. Thus, the external legs in the

processes considered in this paper will always be hard. The situation is different, of course, when studying the damping of soft excitations [17], where at least the incoming particle is soft.

B. Hard sector contribution

The hard sector contribution is calculated as the total transition rate, integrated over the available phase space:

$$\Gamma_h(p) = \frac{1}{2p} \int d\tau_{p'} d\tau_k d\tau_{k'} \overline{|M|^2} (2\pi)^4 \delta^4(P + K - P' - K'). \quad (5)$$

Here, $d\tau_k = d^3k/2k(2\pi)^3$ is the Lorentz invariant phase space volume. When all the particles involved in the scattering process are hard, including the exchanged one, medium effects can be ignored to leading order, and the matrix element is computed with the usual Feynman rules. If the outgoing particles are electrons, the phase space is limited by the Pauli exclusion principle: their energy must be larger than the Fermi energy μ .

Alternatively, we could have chosen to compute the damping rate in a field theoretical approach, as the imaginary part of the self-energy. Generally, the leading hard sector contribution corresponds to the imaginary part of two-loop energy diagrams, as illustrated in Fig. 1 in the case of electron–electron scattering. This equivalence is proven explicitly in Appendix B.

The phase space integration in eq. (5) is easily carried out if an appropriate choice of kinematic variables is made: there are 9 integration variables, and 4 constraints, hence 5 degrees of freedom. Since the transition probability is invariant under a simultaneous rotation of \mathbf{p}' , \mathbf{k} and \mathbf{k}' about the direction of \mathbf{p} , by integrating over this angle only 4 degrees of freedom remain. At this point, it is convenient to introduce the 4-momentum $Q = (\omega, \mathbf{q})$ transferred by the incoming particle to the plasma:

$$Q = (\omega, \mathbf{q}) \equiv P - P' = K' - K \quad (6)$$

We choose 3 variables as k , ω and $q \equiv |\mathbf{q}|$. Note that k and ω fix the energy of the incoming and outgoing particles, while q fixes the angle between \mathbf{k} and \mathbf{k}' . The fourth degree of freedom corresponds to the angle between the plane spanned by $(\mathbf{p}, \mathbf{p}')$ and the plane spanned by $(\mathbf{k}, \mathbf{k}')$ or, equivalently, to the azimuthal angle ϕ of \mathbf{k} around \mathbf{q} . With these variables, eq. (5) becomes

$$\Gamma_h(p) = \frac{1}{128\pi^3 p^2} \int dk d\omega dq \langle |\overline{M}|^2 \rangle \quad (7)$$

where the brackets $\langle \rangle$ denote an average over the azimuthal angle ϕ .

The integration limits on q are easily derived from the definitions in eq. (6):

$$|\omega| < q < \min(k' + k, p' + p) = \min(2k + \omega, 2p - \omega). \quad (8)$$

Since the scattered fermion belongs to the Fermi sea, we have the constraint $k < \mu$. Depending on whether or not the outgoing particles are fermions, additional constraints on k and ω may result from the Pauli blocking conditions: $k' = k + \omega > \mu$ and/or $p' = p - \omega > \mu$. Finally, the momentum transfer is kept hard by imposing $q > q_*$ with $e\mu \ll q_* \ll \mu$. Together with eq. (8), these conditions completely specify the integration domain in eq. (7).

C. Soft sector contribution

When the momentum transfer of a scattering process is of order $e\mu$, one must correct the bare interaction for medium (screening) effects, whose contribution in the propagator is of the same order as the bare propagator itself. This is achieved by replacing the bare propagator by the resummed propagator given in Appendix A. The damping rate is then evaluated as a collision integral similar to eq. (5), however with a screened interaction, as illustrated in Fig. 2 (left) for electron–electron scattering.

The soft contribution to the damping rate can in fact be cast into a much simpler form, as the transition rate of a process where the incoming hard particle, with four-momentum $P = (p, \mathbf{p})$, emits a virtual (spacelike) soft particle with four-momentum $Q = (\omega, \mathbf{q})$ and

scatters into a hard particle with four-momentum $P' = (p', \mathbf{p}')$ (Fig. 2, right). The fact that the soft particle is spacelike means that the actual physical process is, in the example of Fig. 2, electron–electron scattering, not “electron decay”. We show in Appendix B that the two approaches (Fig. 2, left, and Fig. 2, right) are equivalent and amount to evaluate the imaginary part of a (resummed) one–loop self energy diagram (Fig. 2, middle).

The damping rate $\Gamma(p)$, for the process in Fig. 2 (right), can be evaluated from Fermi’s Golden Rule, as in eq. (5), with an important modification: the soft energy ω and momentum $q = |\mathbf{q}|$ are no longer related by a dispersion relation. Instead, a whole range of values are allowed according to a spectral distribution whose actual form is derived from the screening corrections. The damping rate takes then the following form:

$$\Gamma_s(p) = \frac{1}{2p} \int \frac{d^4Q}{(2\pi)^4} \rho(Q) 2\pi\delta((P - Q)^2) \overline{|M|^2}. \quad (9)$$

In this expression, $\rho(Q)$ denotes the spectral function of the soft particle. The spectral function of the outgoing hard particle is simply $2\pi\delta((P - Q)^2)$. $\overline{|M|^2}$ denotes the matrix element of the transition on the right of Fig. 2, squared and summed over final spins, and averaged over the spin states of the incoming particle.

In the limit where q is much softer than p , $(P - Q)^2 = -2p(\omega - q \cos \theta)$, where θ is the angle between \mathbf{q} and \mathbf{p} . Thus the condition that the outgoing hard particle is on its mass shell, $(P - Q)^2 = 0$ reduces to $\cos \theta = \omega/q$. Integrating over θ , the previous equation becomes

$$\Gamma_s(p) = \frac{1}{16\pi^2 p^2} \int_0^{q^*} q dq \int_{-q}^q d\omega \rho(\omega, q) \overline{|M|^2}. \quad (10)$$

Note that $\omega > 0$ (resp. $\omega < 0$) corresponds to the emission (resp. absorption) of a soft particle.

The phase space is further restricted by the Fermi–Dirac and Bose–Einstein distributions, eqs. (B5). If the outgoing hard particle is a fermion, it must be above the Fermi level, which implies $\omega < p - \mu$. If the soft particle is a boson, the only possibility is $\omega > 0$ because there is no boson initially present at $T = 0$. If the soft particle is a fermion, both signs are

possible: $\omega < 0$ corresponds to the absorption of a soft fermion, and $\omega > 0$ to the emission of a soft antifermion. Note that the phase space for the soft virtual particle is limited by the same statistical constraints as if it were a real, on-shell, particle.

It turns out that the matrix element squared $\overline{|M|^2}$ always takes a very simple form, as we shall see in the next section.

III. RESULTS

We now compute explicitly the damping rates of one-particle excitations to leading order in e for the three theories (Yukawa, QED and QCD). We first study the fermionic excitations, in sections III A to III C, then the bosonic excitations, in sections III D and III E. For each type of excitation, we show the self-energy diagrams whose imaginary part corresponds to the elementary process under consideration.

A. Fermion in Yukawa's theory

We consider an incoming fermion of momentum \mathbf{p} above the Fermi level: $p \geq \mu$. In the Yukawa theory, the fermion-fermion scattering matrix element squared, corresponding to the Feynman diagrams depicted in Fig. 3, is a constant given by eq. (2). Collisions are thus dominated by hard momentum transfers, as discussed in section II A. The rate Γ is given by eq. (7), where Fermi statistics imposes the conditions

$$0 < \mu - k < \omega < p - \mu. \quad (11)$$

Using eq. (11), the limits on q given by eqs. (8) reduce to $\omega < q < 2k + \omega$. The integration is straightforward and leads to the expressions

$$\Gamma(p) = \begin{cases} \frac{e^4}{128\pi^3} \frac{\mu^2(3p - 4\mu)}{p^2} & \text{for } p > 2\mu, \\ \frac{e^4}{128\pi^3} \frac{(p - \mu)^2 (4\mu - p)}{p^2} & \text{for } \mu < p < 2\mu. \end{cases} \quad (12)$$

This damping rate corresponds to the imaginary part of the two-loop diagrams displayed in Fig. 4. The third two-loop diagram, the rainbow diagram (see Fig. 7) does not contribute at zero temperature: its imaginary part corresponds to Compton scattering or pair annihilation.

We now consider a hole state (of momentum \mathbf{p} , $p < \mu$). The scattering process is now described in two steps: first an initial vacancy in the Fermi sea is filled by a fermion of momentum \mathbf{p}' ; next the energy difference $p' - p$ is transferred to a fermion of momentum \mathbf{k}' , which is then extracted out of the Fermi sea. Hence, Fermi statistics imposes for this process the conditions $0 < k', p' < \mu < k$. We define ω and q as in eq. (6). Thus eqs. (7) and (8) are still valid. However, eq. (11) is now replaced by

$$p - \mu < \omega < \mu - k < 0. \quad (13)$$

With these conditions, eq. (8) reduces to $-\omega < q < 2p - \omega$. The phase space integration of eq. (7) gives then

$$\Gamma(p) = \frac{3e^4}{128\pi^3} \frac{(\mu - p)^2}{p}. \quad (14)$$

Near the Fermi surface, the damping rate of fermions and holes vanishes quadratically with the excitation energy $|p - \mu|$. We shall come back to this in section IV.

Note that the damping rate diverges for small p . Extrapolating the above formula to the soft domain $p \sim e\mu$ (where our calculation does not apply), one guesses that Γ is of order $e^3\mu$ for a soft excitation, instead of $e^4\mu$ for a hard excitation. A correct calculation shows that it is indeed the case [17].

B. Antifermion in Yukawa's theory

Two collision processes contribute to leading order : Bhabha scattering (Fig. 5 a) and pair annihilation (Fig. 5 b).

The first one gives no difficulty. Its matrix element is

$$\overline{|M|^2} = 2e^4, \quad (15)$$

and the phase space integration goes along the same lines as in section III A, except for the fact that no restriction applies on the final state energy p' . Equation (11) is therefore replaced by

$$0 < \mu - k < \omega. \quad (16)$$

The contribution of Bhabha scattering to the damping rate is then obtained by integrating eq. (7) using eqs. (8) and (16):

$$\Gamma_1(p) = \begin{cases} \frac{e^4}{192\pi^3} p & \text{for } p < \mu, \\ \frac{e^4}{192\pi^3} \frac{\mu^2}{p^2} (3p - 2\mu) & \text{for } p > \mu. \end{cases} \quad (17)$$

For pair annihilation, the tree matrix element is given by eq. (4), and we need to include both hard and soft momentum transfers, according to the discussion following this equation. The hard sector contribution is given by eq. (7). To use this equation, we must average the matrix element over ϕ , the azimuthal angle of \mathbf{k} with respect to \mathbf{q} . We first note that exchanging t and u in eq. (4) amounts to exchanging the two outgoing photons, thus the u/t and t/u terms give identical contributions and $|\overline{M}|^2$ can be replaced by $e^4(u/t - 1)$. From the definition of t and eq. (6), $t = Q^2 = \omega^2 - q^2$. The variable u is given by $u = 2(\mathbf{p} \cdot \mathbf{k}' - pk')$. Decomposing \mathbf{p} and \mathbf{k}' into longitudinal and transverse components with respect to \mathbf{q} , and averaging over ϕ , one gets $\langle \mathbf{p} \cdot \mathbf{k}' \rangle = (\mathbf{p} \cdot \mathbf{q})(\mathbf{k}' \cdot \mathbf{q})/q^2$. From eq. (6), one obtains $\mathbf{p} \cdot \mathbf{q} = \omega p + (q^2 - \omega^2)/2$ and $\mathbf{k}' \cdot \mathbf{q} = \omega k + (q^2 + \omega^2)/2$. The average over ϕ gives therefore $\langle |M|^2 \rangle = e^4(\langle u/t \rangle - 1)$, with

$$\left\langle \frac{u}{t} \right\rangle = \frac{1}{2q^2} \left[(2k + \omega)(2p - \omega) - q^2 \right]. \quad (18)$$

Notice that the collinear divergence (at $\omega \sim \pm q$) canceled out of the ratio.

The limits on q are given by eq. (8), and the only additional restriction from Fermi statistics is $k < \mu$. The integral is logarithmically divergent:

$$\Gamma_{2h}(p) = \frac{e^4 \mu^2}{128\pi^3 p} \left(\log \frac{\mu p}{q_*^2} - \frac{3}{2} \right), \quad (19)$$

where q_* is an IR cutoff for the q -integral.

The soft sector contribution corresponds to pair annihilation “at low angles”, in the sense that the outgoing photons have momenta very close to those of the incoming electron and positron (Fig. 6, left). This can be viewed as a process where a hard antifermion “turns” into a hard boson (see Fig. 6, right) by absorbing a soft fermion ($\omega < 0$) or emitting a soft antifermion ($\omega > 0$). The spectral function of a soft fermion receives contributions from two channels which are labeled by $+$ and $-$ in appendix A. We denote by M_+ and M_- the corresponding matrix elements

$$M_{\pm} = e\bar{u}(\mathbf{p}, \lambda)u(\pm\mathbf{q}, \lambda'). \quad (20)$$

Only states with opposite chiralities have non-vanishing matrix elements, which implies $\lambda' = -\lambda$. Using eq. (A7) and the property that $|\phi_{\mathbf{p}}^{\dagger}\phi_{\hat{\mathbf{q}}}| = \cos(\theta/2)$, θ denoting the angle between \mathbf{p} and \mathbf{q} , one easily obtains the result

$$\sum_{\lambda'} |M_{\pm}|^2 = 2e^2 p(q \mp \omega), \quad (21)$$

where we have used the relation $\cos\theta = \omega/q$. From eqs. (10) and (21), the soft contribution to the damping rate becomes

$$\Gamma_s(p) = \frac{e^2}{8\pi^2 p} \int_0^{q_*} q dq \int_{-q}^q d\omega [(q - \omega)\rho_+(\omega, q) + (q + \omega)\rho_-(\omega, q)], \quad (22)$$

or, by using the relationship $\rho_+(\omega, q) = \rho_-(-\omega, q)$,

$$\Gamma_{2s}(p) = \frac{e^2}{4\pi^2 p} \int_0^{q_*} q dq \int_{-q}^q d\omega (q - \omega) \rho_+(q, \omega). \quad (23)$$

To integrate over ω , we first show the following sum rule:

$$\int_{-\infty}^{\infty} d\omega (q - \omega)\rho_+(q, \omega) = 0. \quad (24)$$

Since ρ_+ is the discontinuity of the Green function G_+ on the real axis, the contour integral in eq. (24) is simply the integral of $(q - z)G_+(q, z)$, with z on a contour going parallel and right above the real axis from $-\infty$ to $+\infty$, and coming back right below it from $+\infty$ to $-\infty$. Deforming the contour into a circle of infinite radius, on which $G_+(q, z)$ reduces to the free

propagator $[2q(z - q)]^{-1}$, one easily sees that the integral vanishes. With the help of the sum rule of eq. (24), one can then express the contribution from the cut piece ($-q < \omega < q$) of the density ρ_+ in eq. (23) in terms of the pole piece ($|\omega| > q$) of the density ρ_+ . The pole contribution to the spectral density is $\rho_+ = 2\pi\delta(G_+^{-1})$. Using eqs. (A8) and (A9), we get

$$\Gamma_{2s}(p) = \frac{e^2}{4\pi^2 p} \int_0^{q_*} q dq \int_{|\omega|>q} d\omega (\omega - q) 2\pi\delta(2q(\omega - q) - \Sigma_+(q, \omega)). \quad (25)$$

Since the mass operator $\Sigma_+(q, \omega)$, given by eq. (A10), depends only on ω/q , it is convenient to change variables from q, ω to $x = \omega/q$ and $y = 2q(\omega - q)$, which gives

$$\Gamma_{2s}(p) = \frac{e^2}{16\pi p} \int \frac{y dx dy}{|x - 1|} \delta(y - \Sigma_+(x)). \quad (26)$$

This can be readily integrated over y and then over x . The integration limits are derived from the dispersion relation eq. (A11). For $q \gg m_f$, one branch is at $x \simeq 1 + m_f^2/q^2$ and the other is at $x \simeq -1$. Thus the integral on x extends from $-\infty$ to -1 and from $1 + m_f^2/q_*^2$ to $+\infty$. One gets

$$\Gamma_{2s}(p) = \frac{e^2 m_f^2}{8\pi p} \left[\log\left(\frac{2q_*^2}{m_f^2}\right) - 2 \right]. \quad (27)$$

Replacing m_f by its value given in Appendix A and adding eqs. (19) and (27), the cutoff q_* cancels out. The contribution of pair annihilation to the damping rate is thus

$$\begin{aligned} \Gamma_2(p) &= \Gamma_{2h}(p) + \Gamma_{2s}(p) \\ &= \frac{e^4 \mu^2}{128\pi^3 p} \left[\log\left(\frac{2\mu p}{m_f^2}\right) - \frac{7}{2} \right] \end{aligned} \quad (28)$$

The total damping rate to order e^4 is the sum of Γ_1 and Γ_2 given by Eqs. (17) and (28). It corresponds to the imaginary part of the self-energy diagrams displayed in Fig. 7. The two-loop diagrams give the hard contribution, while the (resummed) one-loop diagram gives the soft contribution.

C. Fermion and antifermion in QED and QCD

We turn now to studying the fermion lifetime in relativistic QED and QCD plasmas. The damping process is fermion-fermion scattering and is dominated by soft momentum

transfers, as explained in section II B. In QED, we compute this process as the emission of an off-shell soft photon by a hard electron (Fig. 2). The matrix element of the transition is $M = e \bar{u}(\mathbf{p}', \lambda') \gamma^\mu u(\mathbf{p}, \lambda) \epsilon_\mu(\mathbf{q})$, where $\epsilon_\mu(\mathbf{q})$ is the polarization of the photon. Since $q \ll p$, one can replace $\mathbf{p}' = \mathbf{p} - \mathbf{q}$ by \mathbf{p} in the matrix element. Then, the first factor in M is simply the electric current associated with the incoming electron, which reduces to $J^\mu = e \bar{u}(\mathbf{p}, \lambda') \gamma^\mu u(\mathbf{p}, \lambda) = 2e P^\mu \delta_{\lambda, \lambda'}$, the Kronecker symbol reflecting the fact that helicity is conserved in the process. We thus obtain $M = 2e P \cdot \epsilon$. Now, in the Coulomb gauge, the spectral function of the soft photon receives a contribution from longitudinal and transverse modes, which are denoted by $\rho_L(q, \omega)$ and $\rho_T(q, \omega)$ respectively (see Appendix A). The longitudinal polarization vector gives a matrix element $|\overline{M_L}|^2 = 4e^2 p^2$. The two transverse polarization vectors $\epsilon_T^\mu(q, \lambda)$ satisfy $\sum_{\lambda=1,2} \epsilon_T^i(q, \lambda) \epsilon_T^j(q, \lambda) = \delta_{ij} - q_i q_j / q^2$ which gives, upon using $\omega = q \cos \theta$, $|\overline{M_T}|^2 = 4e^2 p^2 (1 - \omega^2 / q^2)$. The soft contribution to the damping rate is given by eq. (10) and the condition $0 < \omega < p - \mu$:

$$\Gamma_s(p) = \frac{e^2}{4\pi^2} \int_0^{q_*} q dq \int_0^{\min(q, p-\mu)} d\omega \left[\rho_L(\omega, q) + \left(1 - \frac{\omega^2}{q^2}\right) \rho_T(\omega, q) \right]. \quad (29)$$

The restriction $\omega > 0$ is due to the conditions $k < \mu$ and $k' > \mu$, which together imply $\omega = k' - k > 0$ (see Fig.2, left). The damping of a hole is calculated in the same manner and leads to the same expression eq. (29), with $p - \mu$ replaced by $\mu - p$.

Since the spectral functions ρ_L and ρ_T fall off rapidly for $q > e\mu$, one can safely take the cutoff q_* to infinity. Introducing then the dimensionless quantities $y = q/q_D$ in eq. (29), $\varepsilon = |p - \mu|/q_D$, and $x = \omega/q$, one obtains

$$\Gamma(\varepsilon) = \frac{e^2 q_D}{4\pi^2} \int_0^1 dx \int_0^{\varepsilon/x} y^2 dy \left[r_L(y, x) + (1 - x^2) r_T(y, x) \right], \quad (30)$$

with $r_{L,T} = q_D^2 \rho_{L,T}$.

In QCD, the damping rate of a quark or a quark hole has a similar expression because the color current of a quark (which enters the matrix element) has the same structure as its electric current. The result is then given by eq. (30) with a multiplicative color factor $C_f = (N_c^2 - 1)/(2N_c)$: $N_c^2 - 1$ for the number of soft gluons, $1/N_c$ for the average over the quark colors and $1/2$ for the trace of SU(3) generator products.

The integrals in eq. (30) can be evaluated numerically. Simple approximate results can be derived in two limits:

1. Far from the Fermi surface, $\varepsilon \gg 1$. As the spectral densities r_L and r_T vanish rapidly for $y \geq 1$, we can extend the upper bound of the y -integral to infinity. One finds

$$\Gamma(p) = 0.057e^2 C_f q_D, \quad (31)$$

or

$$\Gamma(p) = \begin{cases} 0.018e^3 \mu & \text{for QED,} \\ 0.017\sqrt{N_f}e^3 \mu & \text{for QCD with } N_f \text{ flavors, } N_c = 3. \end{cases} \quad (32)$$

2. Very close to the Fermi surface, $\varepsilon \ll 1$. The integration over y covers an appreciable range of values for small values of $x \sim \varepsilon$ only, so that one can safely extend the integral over x to infinity. In the static limit, $x = \omega/q \ll 1$, the longitudinal and transverse spectral functions behave very differently. Static electric fields are screened at distances larger than q_D^{-1} . The longitudinal polarization function, given by eq. (A4), reduces to a constant, $\Pi_L \simeq -q_D^2$, and the corresponding spectral function r_L is

$$r_L = \frac{\pi x}{(y^2 + 1)^2}. \quad (33)$$

Integrating over x first, one finds a contribution to the damping rate of order ε^2

$$\Gamma_L = C_f \frac{e^2 q_D}{4\pi} \int_0^\infty dy \int_0^{\varepsilon/y} dx \frac{xy^2}{(y^2 + 1)^2} + O(\varepsilon^3) \sim C_f \frac{e^2 q_D}{32} \varepsilon^2 + O(\varepsilon^3). \quad (34)$$

On the contrary, the transverse polarization function is purely imaginary for $x \ll 1$, because a static magnetic field is not screened. In this limit ($x = \omega/q \ll 1$), eq. (A5) gives $\Pi_T = -i\pi q_D^2 \omega / 4q^3$, and the spectral function r_T is

$$r_T = \frac{\pi x}{2(y^4 + \pi^2(x/4)^2)}. \quad (35)$$

Even though there is no static screening, the term proportional to x^2 in the denominator induces a deviation from the Rutherford $1/q^4$ (*i.e.* $1/y^4$) behavior, which is referred to as dynamical screening. The main contribution to the damping rate comes from values of y

and x ($x \sim \varepsilon$) such that y^4 and x^2 are of the same order, i.e. such that $q \sim (q_D^2 \omega)^{1/3}$. Upon introducing the variable $y = y' \sqrt{x}/2$ and integrating over x first, one finds

$$C_f \frac{e^2 q_D \varepsilon}{3\pi} \int_0^\infty dy' \frac{y'}{y'^4 + \pi^2} + O(\varepsilon^3) \sim C_f \frac{e^2 q_D}{12\pi} \varepsilon + O(\varepsilon^3). \quad (36)$$

The damping rate is thus dominated by the transverse contribution and gives

$$\Gamma(p) = \begin{cases} \frac{e^2}{12\pi} |p - \mu| & \text{for QED,} \\ \frac{e^2}{9\pi} |p - \mu| & \text{for QCD with } N_f \text{ flavors, } N_c = 3. \end{cases} \quad (37)$$

For the damping rate of a positron or an antiquark, Rutherford scattering has a matrix element varying as $(u/t)^2$ and dominates over pair-annihilation and the s -channel contribution to Bhabha scattering, varying respectively as (u/t) and (u^2/s^2) . The soft sector contribution gives therefore the leading order term. Since the electric and color currents are the same as for electrons or quarks, up to a sign, the damping rate is also given by eq. (30), without the restriction $t < \epsilon/x$ coming from Pauli blocking. The damping rate is then given by the result of eq. (32) for all momenta.

D. Boson in Yukawa's theory and QED

An incident beam (of given central energy) of scalar bosons or photons will undergo a spectral broadening due to the elastic scattering of its quanta with electrons (Compton scattering). The matrix element squared, $\overline{|M|^2}$, corresponding to the diagrams depicted in Fig. 8, is related to that of pair annihilation by crossing symmetry. For a Yukawa interaction, one deduces from eq. (4)

$$\overline{|M|^2} = 2e^4 \left(-\frac{u}{s} - \frac{s}{u} + 2 \right), \quad (38)$$

whereas for a hard photon we have

$$\overline{|M|^2} = 4e^4 \left(-\frac{u}{s} - \frac{s}{u} \right). \quad (39)$$

The computation of the damping rate is similar to the calculation done in section III B. In particular, both hard and soft momentum transfers may contribute.

To compute the hard contribution, we define the variables $\omega = p + k = p' + k'$ and $\mathbf{q} = \mathbf{p} + \mathbf{k} = \mathbf{p}' + \mathbf{k}'$, so that $s = \omega^2 - q^2$. Taking k' , ω and q as integration variables, the contribution to the damping rate is given by eq. (7), with k replaced by k' . The matrix element $|\overline{M}|^2$ must be averaged over the azimuthal angle of \mathbf{k} around \mathbf{q} . Following the same method as for pair annihilation, we obtain an equation similar to eq. (18):

$$\left\langle \frac{u}{s} \right\rangle = \frac{1}{2q^2} [(2k' - \omega)(2p - \omega) - q^2]. \quad (40)$$

The limits on q are $\max(|2p - \omega|, |2k' - \omega|) < q < \omega$, and the constraints from Fermi statistics are $\omega - p < \mu < k'$.

The inverse term ($-s/u$) is integrated using the variables $\omega = k - p' = k' - p$, $\mathbf{q} = \mathbf{k} - \mathbf{k}' = \mathbf{k}' - \mathbf{p}$ and following the same steps as for the direct term.

Adding up the direct and inverse terms, we find for the hard sector contribution to the damping rate of a Yukawa boson

$$\begin{aligned} \Gamma(p < \mu) &= \frac{e^4 p}{192\pi^3} \left[1 - \frac{3\mu^2}{p^2} \log \left(1 - \frac{p^2}{\mu^2} \right) \right] \\ \Gamma(p > \mu) &= \frac{e^4 \mu^2}{64\pi^3 p} \left[3 - \frac{2\mu}{3p} + \log \left(\frac{(p - \mu)p\mu}{(p + \mu)q_*^2} \right) \right]. \end{aligned} \quad (41)$$

For a photon (QED) we obtain

$$\begin{aligned} \Gamma(p < \mu) &= -\frac{e^4 p}{96\pi^3} \left[1 + \frac{3\mu^2}{p^2} \log \left(1 - \frac{p^2}{\mu^2} \right) \right] \\ \Gamma(p > \mu) &= \frac{e^4 \mu^2}{32\pi^3 p} \left[1 + \frac{2\mu}{3p} + \log \left(\frac{(p - \mu)p\mu}{(p + \mu)q_*^2} \right) \right]. \end{aligned} \quad (42)$$

As in section (III B), the logarithmic divergence in q_* corresponds to processes where the intermediate fermion state is soft in the second diagram of Fig. 8. In these processes, the incoming photon (boson) transfers almost all its energy to the outgoing electron. Since the outgoing electron is always above the Fermi level, this situation can occur only if $p > \mu$ (We assume for simplicity that $|p - \mu| \gg e\mu$). Thus the logarithmic divergence is present only for $p > \mu$, as can be seen in eqs. (41) and (42). Then, both soft and hard momentum transfers contribute.

The soft sector contribution corresponds to the emission of a soft antifermion (or to the absorption of a soft fermion) by a hard boson (Fig. 9, right). Since $k' \simeq p$, the corresponding matrix element is approximately given by eq. (20) for a Yukawa boson, and by

$$M_{\pm} = e \bar{u}(\mathbf{p}, \lambda) \boldsymbol{\epsilon}_T \cdot \boldsymbol{\gamma} u(\pm \mathbf{q}, \lambda'), \quad (43)$$

for a QED photon, where $\boldsymbol{\epsilon}_T$ is the polarization vector. Since $\boldsymbol{\epsilon}_T$ is transverse with respect to the photon momentum \mathbf{p} , The operator $\boldsymbol{\epsilon}_T \cdot \boldsymbol{\gamma}$ anticommutes with the Dirac operator $p\gamma^0 - \mathbf{p} \cdot \boldsymbol{\gamma}$ and with the chirality operator γ^5 . Thus, it simply changes $\bar{u}(\mathbf{p}, \lambda)$ into $\bar{u}(\mathbf{p}, -\lambda)$, up to a phase. The matrix element is the same as for the Yukawa interaction. The only difference is that the chirality λ is conserved ($\lambda' = \lambda$), while it changes in the Yukawa theory ($\lambda' = -\lambda$).

In both cases, the resulting soft sector contribution takes therefore the same form as the soft contribution for positron annihilation in eq. (23) with an additional factor 2 for the final electron spins, and with an additional restriction on phase space from Fermi statistics, $p - \omega > \mu$. Since ω is of order $e\mu$, this restriction can be ignored as soon as the boson energy is not too close to the Fermi energy, i.e. if $p - \mu \gg e\mu$. In this condition, the damping rate is given by eq. (27), multiplied by a factor of 2. Adding up the hard and soft contributions, we find for the hard Yukawa boson

$$\begin{aligned} \Gamma(p < \mu) &= \frac{e^4 p}{192\pi^3} \left[1 - \frac{3\mu^2}{p^2} \log \left(1 - \frac{p^2}{\mu^2} \right) \right] \\ \Gamma(p > \mu) &= \frac{e^4 \mu^2}{64\pi^3 p} \left[1 - \frac{2\mu}{3p} + \log \left(\frac{2p\mu(p - \mu)}{m_f^2(p + \mu)} \right) \right], \end{aligned} \quad (44)$$

and for a hard photon

$$\begin{aligned} \Gamma(p < \mu) &= -\frac{e^4 p}{96\pi^3} \left[1 + \frac{3\mu^2}{p^2} \log \left(1 - \frac{p^2}{\mu^2} \right) \right] \\ \Gamma(p > \mu) &= \frac{e^4 \mu^2}{32\pi^3 p} \left[-1 + \frac{2\mu}{3p} + \log \left(\frac{2p\mu(p - \mu)}{m_f^2(p + \mu)} \right) \right]. \end{aligned} \quad (45)$$

Once again the cutoff q_* has canceled out upon addition of the hard and soft contributions. These results are valid only far from the Fermi surface, i.e. for $|p - \mu| \gg e\mu$. The corresponding self-energy diagrams are displayed in Fig. 10.

E. Gluon

Three tree diagrams contribute to Compton scattering of a gluon. They are displayed in Fig. 11. The first, as shown below, yields a contribution of order $e^3\mu$; the contribution from

the other ones is subleading and is of the same order in e as in QED, *i.e.* of order $e^4\mu$ or $e^4\mu \log(1/e)$ (see previous subsection).

The scattering process in Fig. 11, left, can be viewed as the emission of a soft gluon by a hard one (see Fig. 12). The matrix element is evaluated as follows. The three gluon vertex, coupling a hard gluon of color index a , momentum p and polarization ϵ_p to a hard and a soft gluon of color indices b and c , momenta p' and q and polarizations $\epsilon_{p'}$ and ϵ_q respectively, is

$$M = e f^{abc} (\epsilon_p \cdot \epsilon_{p'} (P + P') \cdot \epsilon_q + \epsilon_{p'} \cdot \epsilon_q (-P' + Q) \cdot \epsilon_p + \epsilon_q \cdot \epsilon_p (-Q - P) \cdot \epsilon_{p'}), \quad (46)$$

where f^{abc} is the $SU(3)$ structure constant. The hard gluons are on-shell transverse gluons, whose polarization vectors satisfy $\epsilon_p \cdot P = \epsilon_{p'} \cdot P' = 0$. Therefore, in the limit $q \ll p$, the last two terms in eq. (46) vanish. The remaining term is

$$M = 2e f^{abc} (\epsilon_p \cdot \epsilon_{p'}) (P \cdot \epsilon_q). \quad (47)$$

This can be written in the form $M = J_\mu \epsilon_q^\mu$ where $J_\mu = 2e f^{abc} (\epsilon_p \cdot \epsilon_{p'}) P_\mu$ is the matrix element of the color current between the initial and final hard gluon states. In this form, it is analogous to the matrix element obtained in the case of the emission of a soft photon by a hard electron (see section III C).

The gluon damping rate is therefore given by an equation similar to eq. (29), with two minor modifications: the condition $\omega < p - \mu$ does not apply for a final gluon state, and the result must be multiplied by a factor $N_c/2 = f_{abc} f_{abc}/16$ coming from the color degrees of freedom: N_c for the possible ways of transferring color to the soft gluons, and $1/2$ for the symmetry factor. For $N_c = 3$, the numerical value is

$$\begin{aligned} \Gamma(p) &= \frac{3}{2} 0.057 e^2 q_D, \\ &= 0.019 \sqrt{N_f} e^3 \mu. \end{aligned} \quad (48)$$

IV. DISCUSSION

Damping rates of hard particles in a cold ultrarelativistic fermion gas are at least of order e^3 higher than their energy: hence, one-particle excitations are narrow quasiparticle

states in the perturbative regime $e \ll 1$. The damping rates of the various one-particle excitations are displayed as a function of their momentum p in Figs. 14, 15 and 16 for the Yukawa interaction, QED and QCD respectively.

We distinguish two categories of damping processes: for charged particles in gauge theories, the scattering process is essentially forward ($\theta \sim e$) and the resulting damping rate is of order $e^3\mu$; for other particles, large angle scattering ($\theta \sim 1$) contributes at least as much as small angle scattering, and the damping rate is of order $e^4\mu$ or $e^4\mu \log(1/e)$. Notice that the results derived in sections III C, III D and III E are gauge invariant: all the matrix elements used in either the hard or the soft sector contributions are averaged over physical polarization states.

A. Damping rates of charged particles in gauge theories

Damping rates of charged particles are dominated by collisions with soft momentum transfer, for which medium effects must be taken into account: scattering takes place through the coupling of the elementary particle current with coherent plasma oscillations of the charge and current densities. The underlying classical structure is clear: the transition rate depends on the hard particle only through the associated current. We are in a situation where the hard particle motion is only slightly perturbed by the soft one: the gauge field behaves essentially as a classical field which couples to the current of the hard particles.

The electron and quark damping rates are very similar, in the sense that they differ only by trivial color factors. On the other hand, the gluon and photon damping processes are essentially different: the dominant contribution to gluon damping involves the three-gluon vertex (see Fig. 11), and the damping rate Γ is of order $e^3\mu$, as for electrons and quarks. Gluon damping is therefore specifically non-abelian. The photon damping rate is smaller in magnitude, of order $e^4\mu \log(1/e)$ or $e^4\mu$.

It is interesting to note that the damping rates of charged particles are independent of the particle momentum. The only exception comes from electrons or quarks very close

to the Fermi surface, within an interval $e\mu$ from the Fermi level, where the damping rate decreases with the excitation energy $|p - \mu|$ (section III C). Then, the longitudinal part of the interaction is screened at low momenta and leads to a width *quadratic* in $|p - \mu|$. The dominant term, shown in eq. (37), is the contribution from the transverse piece of the interaction, which is not screened in the static limit, and the width is *linear* in $|p - \mu|$. This correlation between the range of interaction and the electron damping rate close to the Fermi surface is already well-known in the non-relativistic electron gas ([19] and [20]). In particular, our result of eq. (37) agrees with the energy dependence of the imaginary part of the electron self-energy derived in [20], if we set the Fermi velocity $v_F = p_F/m$ to $v_F = 1$.

Note that the calculation presented here is valid only for hard momentum excitations. The damping of soft, charged, excitations in gauge theories has very different properties: first, it is momentum dependent; second, the hard contribution is no longer negligible, but becomes of the same order of magnitude as the soft contribution, yielding a damping rate of order $e^3\mu \log(1/e)$, instead of $e^3\mu$ for hard excitations [17].

B. Damping rates of other particles

Other particles include neutral particles (photons, Yukawa scalars) and fermions with a Yukawa coupling, for which the interaction $\phi\bar{\psi}\psi$ is not related to any conserved charge. For these particles, the hard contribution to the damping rate is at least of the same order of magnitude as the soft contribution. While the soft contribution involves medium effects, i.e. coherent effects, the hard contribution simply results from incoherent collisions: a quasiparticle excitation dies off by kicking electrons out of the Fermi sea randomly. The resulting damping rates are smaller in magnitude, of order $e^4\mu$ or $e^4\mu \log(1/e)$. They are strongly momentum dependent, as can be seen in Figs. 14 and 15.

The $\log(1/e)$ term comes from processes in which a massless fermion is exchanged, and the fermion propagator must be corrected for medium effects. These processes are specific to relativistic plasmas. As a result of the medium effects, the photon and the scalar boson

damping rates are strongly momentum dependent: they rise steeply near the Fermi energy (see Figs. 14 and 15), and are of order $e^4\mu$ for $p < \mu$ and $e^4\mu \log(1/e)$ for $p > \mu$. Once again, the soft momentum transfer process is almost classical in nature. Here, it is the fermionic soft field which acts as a classical field (recall that the dispersion relation of soft fermions is the same for both interactions) in which the hard particles move [21].

Near the Fermi surface, the fermion damping rate in a Yukawa theory decreases *quadratically* with $|p - \mu|$, in contrast with the electron and quark damping rates. This is a consequence of the fact that hard momentum transfers dominate and that in this sense, the interaction is short-ranged.

Damping rates of soft excitations are of order $e^3\mu$ or $e^3\mu \log(1/e)$, i.e. one power in e smaller than for hard momenta. The additional factor $1/e$ comes from kinematics [17].

C. Comparison with the high temperature case

As noted in the introduction, ultrarelativistic plasmas have the same screening properties in the high density ($T = 0$) and high temperature ($\mu = 0$) limits. For neutral particles, we have seen that damping rates are of order $e^4\mu$ or $e^4\mu \log(1/e)$ at $T = 0$. These damping rates are generally of order $e^4T \log(1/e)$ at high temperature [22]. The $\log(1/e)$ factor comes from processes in which a soft fermion is exchanged, i.e. Compton scattering and pair annihilation at low angles. At $T = 0$, these processes are not always possible (see sections III A and III D) and the $\log(1/e)$ then disappears. Apart from this difference, the orders of magnitude of damping rates are the same in the hot and cold plasmas.

For charged particles, the situation is very different. Naive perturbation theory yields an infrared divergent damping rate in the $T = 0$ ($\mu > 0$) and $\mu = 0$ ($T > 0$) limits. However, the level of divergence is different in these two cases, because screening at the one-loop level gives a finite damping rate, of order $e^3\mu$, if $T = 0$, whereas in the high temperature case the damping rate is logarithmically divergent and of order e^2T . In both cases, the damping processes are elastic collisions with the charges in the plasma. The

essential difference lies in Pauli blocking: at zero temperature, processes in which a boson with energy $\omega \sim e\mu$ is exchanged have a phase space proportional to ω (only electrons very close to the Fermi surface participate in the collisions), whereas at high temperature, phase space is proportional to T . This factor ω both contributes a factor e and kills the divergence at $\omega = 0$.

ACKNOWLEDGMENTS

After completion of this work, we learned that M. le Bellac and C. Manuel have recently calculated the damping rates of electrons and holes near the Fermi surface in QED and QCD [23]. We have benefited from discussions with a number of people. It is a pleasure to thank J.P. Blaizot and E. Iancu for useful comments on the manuscript as well as G. Baym for helpful remarks. This work has been supported in part by the US National Science Foundation under Grant NSF PHY94-21309.

APPENDIX A: SPECTRAL DENSITIES OF SOFT MODES

In this appendix, we recall how boson and fermion propagators at low momenta are modified by medium effects in an ultrarelativistic plasma.

1. Soft gauge field

In the Coulomb gauge, rotational invariance allows one to decompose the photon propagator into a longitudinal (L) and a transverse (T) piece [24]:

$$D^{\mu\nu}(\mathbf{q}, z) = D_L(q, z)\epsilon_L^\mu\epsilon_L^\nu + D_T(q, z)\sum_{\lambda=1,2}\epsilon_T^\mu(\mathbf{q}, \lambda)\epsilon_T^\nu(\mathbf{q}, \lambda) \quad (\text{A1})$$

where $\epsilon_L^\mu = \delta_0^\mu$ and $\epsilon_T^\mu(\mathbf{q}, \lambda)$, $\lambda = 1, 2$, are spacelike unit vectors mutually orthogonal and transverse to \mathbf{q} , therefore satisfying $\sum_{\lambda=1,2}\epsilon_T^i(\mathbf{q}, \lambda)\epsilon_T^j(\mathbf{q}, \lambda) = \delta_{ij} - q_i q_j / \mathbf{q}^2$. For the bare QED interaction, the decomposition of the propagator $D_0^{\mu\nu}(q, z)$ according to eq. (A1) gives

$$D_{0L}^{-1}(q, z) = q^2; \quad D_{0T}^{-1}(q, z) = z^2 - q^2. \quad (\text{A2})$$

For soft momenta $q \sim e\mu$, the propagator is modified by medium effects:

$$D_{\mu\nu}^{-1}(q, z) = D_{0,\mu\nu}^{-1}(q, z) - \Pi_{\mu\nu}(q, z). \quad (\text{A3})$$

To leading order in e^2 , the polarization tensor $\Pi_{\mu\nu}(q, z)$ is given by bubble diagrams corresponding to the photon coupling to electron–hole intermediate states. Decomposing $\Pi_{\mu\nu}$ according to eq. (A1), one gets ($\eta \rightarrow +0$) [25,26]:

$$\frac{1}{q_D^2} \Pi_L(q, \omega + i\eta) = -1 + \frac{\omega}{2q} \left[\log \left| \frac{\omega + q}{\omega - q} \right| - i\pi\theta(q^2 - \omega^2) \right], \quad (\text{A4})$$

$$\frac{1}{q_D^2} \Pi_T(q, \omega + i\eta) = \frac{\omega^2}{2q^2} + \frac{\omega(q^2 - \omega^2)}{4q^3} \left[\log \left| \frac{\omega + q}{\omega - q} \right| - i\pi\theta(q^2 - \omega^2) \right]. \quad (\text{A5})$$

Notice that the full one–loop self–energy contains also diagrams corresponding to electron–positron intermediate states, however their self–energies are a power of e smaller than those of eqs. (A4), (A5), see [25,26]. In eqs. (A4), (A5), q_D is the Debye screening momentum, given by the first entry of the following table. The resummed propagator obtained from eqs. (A3–A5) is drawn as a photon propagator with a “blob” (see for instance Fig. 2).

The gluon propagator and gluon self–energy are diagonal in color indices, which we omit for brevity. In the strict Coulomb gauge, in the sense defined in the second reference of [11], the decomposition (A1) holds for the gluon propagator, and eqs. (A1) through (A5) remain valid. The Debye screening momentum q_D is given by the second entry of the following table.

Theory	q_D
QED	$e\mu/\pi$
QCD	$e\mu\sqrt{N_f}/(\pi\sqrt{2})$

The spectral density $\rho^{\mu\nu}(\mathbf{q}, \omega) = -2 \text{Im} D^{\mu\nu}(\mathbf{q}, \omega + i\eta)$, ($\eta \rightarrow +0$) can be decomposed, like the propagator in eq. (A1), into longitudinal and transverse pieces, $\rho_{L,T}(q, \omega) = -2 \text{Im} D_{L,T}(q, \omega + i\eta)$. Their expressions are easily obtained from eqs. (A2–A5). For free fields, they reduce to $\rho_{0L}(q, \omega) = 0$, $\rho_{0T}(q, \omega) = 2\pi\delta(\omega^2 - q^2)(\theta(\omega) - \theta(-\omega))$: the only peaks

are at $\omega = \pm q$ and correspond to transverse photons (gluons). For soft momenta, ρ_L and ρ_T are modified by medium effects. The peaks of ρ_T are shifted towards higher values of $|\omega|$, and a peak appears in ρ_L at the values of ω given by $D_{0,L}^{-1}(q, \omega) - \Pi_L(q, \omega) = 0$, corresponding to plasmon modes. Note that the real parts of $D_{L,T}^{-1}(q, \omega)$ are even in ω for fixed q , so that the peaks always appear in pairs of opposite sign $\pm\omega$. In addition to these peaks, the spectral densities have a continuous part for $|\omega| < q$ coming from the imaginary part of the polarization in eqs. (A4–A5), which corresponds physically to Landau damping: waves with $|\omega| < q$ lose their energy by accelerating fermions.

2. Soft fermion

The fermion propagator can be decomposed on a basis of spinors in the following way (once again, we omit trivial color indices for the quark propagator):

$$G(\mathbf{p}, z) = G_+(p, z) \sum_{\lambda=-1,1} u(\mathbf{p}, \lambda) \bar{u}(\mathbf{p}, \lambda) + G_-(p, z) \sum_{\lambda=-1,1} u(-\mathbf{p}, \lambda) \bar{u}(-\mathbf{p}, \lambda). \quad (\text{A6})$$

In this decomposition, $u(\mathbf{p}, \lambda)$ denotes a solution of the free massless Dirac equation $(p\gamma^0 - \mathbf{p} \cdot \boldsymbol{\gamma})u(\mathbf{p}, \lambda) = 0$ with chirality λ , normalized according to the relation $\sum_{\lambda=-1,1} u(\mathbf{p}, \lambda) \bar{u}(\mathbf{p}, \lambda) = p\gamma^0 - \mathbf{p} \cdot \boldsymbol{\gamma}$. Note that $u(\mathbf{p}, \lambda)$ is a positive energy solution, while $u(-\mathbf{p}, \lambda)$ is the corresponding negative energy solution with the same momentum \mathbf{p} : it corresponds to a positron (or an antiquark) with momentum $-\mathbf{p}$. An explicit expression of $u(\mathbf{p}, \lambda)$ is most easily obtained in the chiral representation of Dirac matrices:

$$u(\mathbf{p}, +1) = \sqrt{2p} \begin{pmatrix} \phi_{\hat{\mathbf{p}}} \\ 0 \end{pmatrix} \quad u(\mathbf{p}, -1) = \sqrt{2p} \begin{pmatrix} 0 \\ \phi_{-\hat{\mathbf{p}}} \end{pmatrix} \quad (\text{A7})$$

where $\hat{\mathbf{p}} \equiv \mathbf{p}/p$ and $\phi_{\hat{\mathbf{p}}}$ is a two component spinor pointing in the direction of $\hat{\mathbf{p}}$, i.e. satisfying $\boldsymbol{\sigma} \cdot \hat{\mathbf{p}} \phi_{\hat{\mathbf{p}}} = \phi_{\hat{\mathbf{p}}}$, normalized to unity $\phi_{\hat{\mathbf{p}}}^\dagger \phi_{\hat{\mathbf{p}}} = 1$. Note that $\phi_{\hat{\mathbf{p}}} \phi_{\hat{\mathbf{p}}}^\dagger = (1 + \boldsymbol{\sigma} \cdot \hat{\mathbf{p}})/2$

For the free Dirac propagator $G_0^{-1}(\mathbf{p}, z) = z\gamma^0 - \mathbf{p} \cdot \boldsymbol{\gamma}$, the decomposition (A6) gives

$$G_{0\pm}^{-1}(p, z) = 2p(z \mp p). \quad (\text{A8})$$

As expected, the poles of G_+ and G_- are respectively the positive and negative energy solution of the free Dirac equation. For soft momenta $p \sim e\mu$, the fermion propagator is corrected by medium effects:

$$G^{-1}(p, z) = G_0^{-1}(p, z) - \Sigma(p, z). \quad (\text{A9})$$

The mass operator $\Sigma(p, z)$ can be decomposed according to eq. (A6), so that $G_{\pm}^{-1} = G_{0\pm}^{-1} - \Sigma_{\pm}$. To leading order in e^2 , the components Σ_{\pm} are given by ($\eta \rightarrow +0$) [27,28]

$$\begin{aligned} \frac{1}{2m_f^2} \Sigma_+(p, \omega + i\eta) &= 1 - \frac{\omega - p}{2p} \left[\log \left| \frac{\omega + p}{\omega - p} \right| - i\pi\theta(p^2 - \omega^2) \right], \\ \Sigma_-(p, \omega + i\eta) &= -\text{Re} \Sigma_+(p, -\omega + i\eta) + i \text{Im} \Sigma_+(p, -\omega + i\eta). \end{aligned} \quad (\text{A10})$$

The self-energy functions Σ_{\pm} only include the coupling of the soft external fermion to intermediate fermion states through the absorption or the emission of a boson. These terms are the dominant ones for a soft external fermion [27,28]. The quantity m_f in eq. (A10) is the quasiparticle rest energy and is given in the following table:

Theory	m_f
Yukawa	$e\mu/(4\pi)$
QED	$e\mu/(\pi\sqrt{8})$
QCD	$e\mu/(\pi\sqrt{6})$

The spectral density $\rho_F(\mathbf{p}, \omega) = -2 \text{Im} G(\mathbf{p}, \omega + i\eta)$ can be decomposed like the propagator in eq. (A6), with $G_{\pm}(p, z)$ replaced by the corresponding spectral density $\rho_{\pm}(p, \omega) = -2 \text{Im} G_{\pm}(p, \omega + i\eta)$. For a free Dirac field, the spectral density reduces to $\rho_{\pm}(p, \omega) = 2\pi\delta(\omega^2 - p^2)\theta(\pm\omega)$. Medium effects modify the spectral density for soft momenta. The position of the peaks of ρ_+ are the solutions of $G_+^{-1}(p, \omega) = 0$. Using eqs. (A8–A10), one obtains the dispersion relation in terms of the parameter $x \equiv \omega/p$:

$$\begin{aligned} \frac{p^2}{m_f^2} &= \frac{1}{x-1} - \frac{1}{2} \log \left(\frac{x+1}{x-1} \right), \\ \omega &= px. \end{aligned} \quad (\text{A11})$$

There are two peaks for a given p . One with $x > 1$, which corresponds to the bare fermion state slightly shifted by its interaction with the medium. Furthermore, a second peak appears for $x < -1$. It corresponds to a new fermionic excitation called “plasmino” which has no counterpart in non-relativistic plasmas. Finally, ρ_+ has a continuous part in the region $|\omega| < p$, which corresponds to the fermionic analogue of Landau damping. The density ρ_- has the same properties, with ω replaced by $-\omega$.

APPENDIX B: SELF-ENERGY DIAGRAMS AND CUTTING RULES

We show explicitly that the kinetic theory approach used in this paper is equivalent to the approach using the formalism of field theory. In field theory, the damping rate $\Gamma(p)$ is defined from the imaginary part of the self energy. In the case of a fermion, using the notations of Appendix A, this relation reads ($\eta \rightarrow +0$) [29]

$$\Gamma(p) = -2 \operatorname{tr} [\not{p} \operatorname{Im} \Sigma(\mathbf{p}, p + i\eta)] / 4p = -2 \operatorname{Im} \Sigma_+(\mathbf{p}, p + i\eta). \quad (\text{B1})$$

Cutting rules (see for example [30]) allow to express the imaginary part of a generic self-energy diagram as the rate of a scattering process, thus providing the equivalence with the kinetic theory approach used in this paper. We show in this appendix that the hard contribution to the damping rate corresponds to a two-loop self energy diagram where the loop momenta are hard (see Fig. 1) while the soft contribution corresponds to a one-loop self-energy diagram with a soft internal momentum (Fig. 2). We take the example of electron-electron scattering in QED. Our arguments can be easily extended to other scattering processes.

We proceed as follows: we first show that the imaginary part of the one-loop resummed diagram depicted in Fig. 17 corresponds to the probability to emit a soft photon (second equality in Fig. 2). Then we show the equality displayed in Fig. 1, i.e. that the rate of electron-electron scattering corresponds to the imaginary part of a two-loop self-energy diagram. Note, however, that the interference term between the two Feynman diagrams of

electron–electron scattering (Fig. 3, right) is not included here. It corresponds to the imaginary part of another two–loop diagram (Fig. 4, right). Finally, we show that the imaginary part of the one–loop resummed diagram corresponds to electron–electron scattering with a resummed interaction (first equality in Fig. 2).

1. One soft loop

The contribution of the diagram in Fig. 17 to the fermion self–energy is given by

$$\Sigma(\mathbf{p}, z_p) = \int \frac{d^3q}{(2\pi)^3} \int_{-i\infty}^{+i\infty} \frac{dz_q}{2i\pi} (-ie\gamma^\mu) G_0(\mathbf{p} - \mathbf{q}, z_p - z_q) (-ie\gamma^\nu) D_{\mu\nu}(\mathbf{q}, z_q). \quad (\text{B2})$$

In this expression, $z_p = \mu + ix$ with x real, G_0 is the fermion propagator, which coincides with the free propagator (A8) for a hard fermion, and D is the soft photon propagator given by eqs. (A3–A5). We write the internal propagators using the spectral representations:

$$\begin{aligned} D_{\mu\nu}(\mathbf{q}, z_q) &= \int_{-\infty}^{+\infty} \frac{d\omega_q}{2\pi} \frac{\rho_{\mu\nu}(\mathbf{q}, \omega_q)}{z_q - \omega_q}, \\ G_0(\mathbf{p}', z_{p'}) &= \int_{-\infty}^{+\infty} \frac{d\omega_{p'}}{2\pi} \frac{\rho_F(\mathbf{p}', \omega_{p'})}{z_{p'} - \omega_{p'}}, \end{aligned} \quad (\text{B3})$$

with $z_q = ix$, $z_{p'} = \mu + ix$ and $\mathbf{p}' = \mathbf{p} - \mathbf{q}$. A straightforward contour integration gives for the integral over z_q :

$$\int_{-i\infty}^{+i\infty} \frac{dz_q}{2i\pi} \frac{1}{z_q - \omega_q} \frac{1}{z_p - z_q - \omega_{p'}} = -\frac{1 + n(\omega_q) - f(\omega_{p'})}{z_p - \omega_q - \omega_{p'}}, \quad (\text{B4})$$

where we have introduced the Bose–Einstein and Fermi–Dirac distribution functions $n(\omega)$ and $f(\omega)$ which, in the limit $T = 0$, reduce to

$$\begin{aligned} n(\omega) &= \frac{1}{e^{\omega/T} - 1} = \theta(\omega) - 1, \\ f(\omega) &= \frac{1}{e^{(\omega-\mu)/T} + 1} = \theta(\mu - \omega). \end{aligned} \quad (\text{B5})$$

After analytic continuation of z_p to $\omega_p + i\eta$, the imaginary part of eq. (B4) becomes

$$\pi\delta(\omega_p - \omega_q - \omega_{p'}) (1 + n(\omega_q) - f(\omega_{p'})). \quad (\text{B6})$$

The imaginary part of the self-energy can thus be obtained from eq. (B2) through replacing the internal propagators by their spectral functions and the Matsubara frequencies z by real frequencies ω , and multiplying by the occupation factor from eq. (B6):

$$-2 \operatorname{Im} \Sigma(\mathbf{p}, p + i\eta) = \int \frac{d^4 Q}{(2\pi)^4} (e\gamma^\mu) \rho_F(P - Q) (e\gamma^\nu) \rho_{\mu\nu}(Q) \times (1 + n(\omega_q) - f(\omega_p - \omega_q)), \quad (\text{B7})$$

where we have introduced the four vectors $P = (p, \mathbf{p})$ and $Q = (\omega_q, \mathbf{q})$, and $\omega_p = p$.

Note that the occupation factors can be rewritten as

$$1 + n(\omega_q) - f(\omega_{p'}) = (1 + n(\omega_q))(1 - f(\omega_{p'})) + n(\omega_q)f(\omega_{p'}). \quad (\text{B8})$$

The two terms correspond to the amplitudes for the direct and inverse process in Fig. 2 (right). If $\omega_p > \mu$ (particle excitation), only the direct process contributes, when $0 < \omega_q < \omega_p - \mu$. If $\omega_p < \mu$ (hole excitation), on the other hand, only the inverse process contributes, when $\mu - \omega_p < \omega_q < 0$. Note that in this last case, the occupation factor is $nf = -1$; however, the boson spectral function also has an opposite sign for $\omega_q < 0$ (see eqs. (A4-A5)) so that the global sign is unchanged.

Decomposing the spectral functions according to eqs. (A1) and (A6), and taking into account that $\rho_+(p, \omega) = 2\pi\delta(\omega^2 - p^2)\theta(\omega)$ for a hard fermion (the spectral function is the same as in the vacuum, and ρ_- does not contribute since $\omega_p - \omega_q > 0$), one obtains from eq. (B7):

$$-2 \bar{u}(\mathbf{p}, \lambda) \operatorname{Im} \Sigma(\mathbf{p}, p + i\eta) u(\mathbf{p}, \lambda) = \int \frac{d^4 Q}{(2\pi)^4} 2\pi\delta((P - Q)^2) \sum_{j=L,T} \rho_j(Q) \sum_{\lambda'} |M_j|^2 \times (1 + n(\omega_q) - f(\omega_p - \omega_q)). \quad (\text{B9})$$

where M_j is the matrix element of the transition process in Fig. 2 (right):

$$M_j = \bar{u}(\mathbf{p}', \lambda') (-ie\gamma_\mu) u(\mathbf{p}, \lambda) \epsilon_j^\mu(\mathbf{q}). \quad (\text{B10})$$

Comparing eq. (B9) with eq. (9), one concludes

$$\Gamma(p) = -2 \bar{u}(\mathbf{p}, \lambda) \operatorname{Im} \Sigma(\mathbf{p}, p + i\eta) u(\mathbf{p}, \lambda) / 2p, \quad (\text{B11})$$

$$= -2 \operatorname{tr} [\not{p} \operatorname{Im} \Sigma(\mathbf{p}, p + i\eta)] / 4p. \quad (\text{B12})$$

2. Two hard loops

We now turn to the second step: we show that the imaginary part of the two-loop diagram on the right of Fig. 1 corresponds to the rate of electron–electron scattering with the diagram on the left of Fig. 1. The contribution of the two-loop diagram to the self-energy is given by a formula analogous to eq. (B2), where D is replaced by a photon line with a fermion loop insertion, i.e. by $D_0\Pi D_0$, with

$$\Pi^{\mu\nu}(\mathbf{q}, z_q) = \int \frac{d^3k}{(2\pi)^3} \int_{\mu-i\infty}^{\mu+i\infty} \frac{dz_k}{2i\pi} \text{tr} [G_0(\mathbf{k}, z_k)(e\gamma^\mu)G_0(\mathbf{k} + \mathbf{q}, z_k + z_q)(e\gamma^\nu)] \quad (\text{B13})$$

with z_q on the imaginary axis. Therefore, the imaginary part of the two-loop diagram is given by eq. (B7), in which the boson spectral function $\rho(\mathbf{q}, \omega_q) = -2 \text{Im} D(\mathbf{q}, \omega_q + i\eta)$ is replaced by $-2 \text{Im}(D_0\Pi D_0)$. Now, the imaginary part of D_0 vanishes because both fermions are on mass shell ($|\omega_p| = p$ and $|\omega_p - \omega_q| = |\mathbf{p} - \mathbf{q}|$), which implies $|\omega| < q$. Thus we can write $\text{Im}(D_0\Pi D_0) = D_0(\text{Im}\Pi)D_0$. To calculate $\text{Im}\Pi$, we follow the same steps as for $\text{Im}\Sigma$ in eq. (B2). Using the spectral representation to write the internal propagators, the integral over z_k can be calculated easily ($\mathbf{k}' = \mathbf{k} + \mathbf{q}$):

$$\int_{\mu-i\infty}^{\mu+i\infty} \frac{dz_k}{2i\pi} \frac{1}{z_k - \omega_k} \frac{1}{z_k + z_q - \omega_{k'}} = \frac{f(\omega_k) - f(\omega_{k'})}{z_q + \omega_k - \omega_{k'}}. \quad (\text{B14})$$

After analytic continuation of z_q to $\omega_q + i\eta$, the imaginary part of this equation becomes

$$- \pi \delta(\omega_q + \omega_k - \omega_{k'}) (f(\omega_k) - f(\omega_{k'})). \quad (\text{B15})$$

One thus obtains

$$\begin{aligned} -2 \text{Im} \Pi^{\mu\nu}(\mathbf{q}, \omega_q + i\eta) &= \int \frac{d^3k}{(2\pi)^3} \frac{d\omega_k}{2\pi} \text{tr} [\rho_F(\mathbf{k}, \omega_k)(e\gamma^\mu)\rho_F(\mathbf{k} + \mathbf{q}, \omega_k + \omega_q)(e\gamma^\nu)] \\ &\quad \times (f(\omega_k) - f(\omega_{k'})). \end{aligned} \quad (\text{B16})$$

Replacing ρ in eq. (B7) by $-2D_0(\text{Im}\Pi)D_0$, using eq. (B16), and decomposing the fermion spectral functions according to eq. (A6), one obtains

$$\begin{aligned} \Gamma(p) &= \frac{1}{2p} \int \frac{d^4Q}{(2\pi)^4} \int \frac{d^4K}{(2\pi)^4} (2\pi)\delta((P - Q)^2) (2\pi)\delta(K^2) (2\pi)\delta((K + Q)^2) |M|^2 \\ &\quad \times (f(\omega_k) - f(\omega_{k'}))(1 + n(\omega_q) - f(\omega_{p'})). \end{aligned} \quad (\text{B17})$$

where $K = (\omega_k, \mathbf{k})$. Notice that, from $K^2 = 0$, the only possible solution for ω_k is $\omega_k = k$, only electrons are initially present in the Fermi sea. The matrix element M is given by $M = \sum_{\lambda', \kappa, \kappa'} J_{p', \lambda'; p, \lambda}^\mu J_{k', \kappa'; k, \kappa \mu} (1/Q^2)$ with $J_{p', \lambda'; p, \lambda}^\mu = e \bar{u}(p', \lambda') \gamma^\mu u(p, \lambda)$ and corresponds indeed to the direct contribution to electron–electron scattering (Fig. 1, left). Introducing the four vectors $K' = K + Q$ and $P' = P - Q$, integrating over Q and making use of the identity $\int (d^4 K)/(2\pi)^4 2\pi \delta(K^2) \Theta(K_0) = \int d\tau_k$, one finds eq. (5), up to the statistical factors. Thus, we only need to check that the product of the phase space factors eq. (B6) and (B15) corresponds to electron–electron scattering. For this purpose, we note that the energy conservation $\omega_q + \omega_k = \omega_{k'}$ implies the following relations between the statistical factors:

$$\begin{aligned} n(\omega_q) (f(\omega_k) - f(\omega_{k'})) &= (1 - f(\omega_k)) f(\omega_{k'}) \\ (1 + n(\omega_q)) (f(\omega_k) - f(\omega_{k'})) &= (1 - f(\omega_{k'})) f(\omega_k) \end{aligned} \quad (\text{B18})$$

Using these equations together with eq. (B8), one obtains immediately the phase space factor under the form

$$(1 - f(\omega_{p'})) f(\omega_k) (1 - f(\omega_{k'})) + f(\omega_{p'}) (1 - f(\omega_k)) f(\omega_{k'}). \quad (\text{B19})$$

The two terms correspond to the amplitudes of the direct and inverse process, as expected.

3. Screened interaction

Finally, we show that the imaginary part of the one loop resummed diagram corresponds to the probability of electron–electron scattering with a screened interaction (first equality in Fig. 2). This is a straightforward extension of the previous result. We start from eq. (B7). The spectral function of the resummed photon line, ρ , is given by $\rho = -2\text{Im}D = 2|D|^2(\text{Im}D^{-1})$. Using eq. (A3) and the fact that $\text{Im}D_0^{-1} = 0$, as discussed above, one obtains $\rho = -2|D|^2(\text{Im}\Pi)$. Thus the only difference with the previous case is that the free photon propagator D_0 is replaced by the resummed photon propagator D , which includes the screening effects.

REFERENCES

- [1] M.H. Thoma, *Applications of High-Temperature Field Theory to Heavy-Ion Collisions in Quark-Gluon plasma 2*, Editor R.C. Hwa (World Scientific, 1996), and references therein. J.P. Blaizot, J.-Y. Ollitrault and E. Iancu, *Collective Phenomena in the Quark-Gluon Plasma*, *ibid.*
- [2] B. A. Freedman and L. D. McLerran, Phys. Rev. **D16** (1977) 1130; Phys. Rev. **D16** (1977) 1147; Phys. Rev. **D16** (1977) 1169.
- [3] J-P. Blaizot and J-Y. Ollitrault, Phys. Rev. **D48** (1993) 1390.
- [4] H. Vija and M. H. Thoma, Phys. Lett. **B342** (1995) 212; C. Manuel, Phys. Rev. **D53** (1996) 5866.
- [5] A. Rosenhauer *et al.*, Nucl. Phys. **A540** (1992) 630.
- [6] P. Braun-Munzinger *et al.*, Phys. Lett. **B344** (1995) 43; Phys. Lett. **B365** (1996) 1.
- [7] E. Braaten, Phys. Rev. Lett. **74** (1995) 2164; E. Braaten and A. Nieto, Phys. Rev. **D51** (1995) 6990.
- [8] F. Flechsig, H. Schulz and A.K. Rebhan, Phys. Rev. **D52**(1995) 2994.
- [9] G. Baym, H. Monien, C.J. Pethick and D.J. Ravenhall, Phys. Rev. Lett. **64** (1990) 1867.
- [10] E. Braaten and M.H. Thoma, Phys. Rev. **D44** (1991) 2625.; Phys. Rev. **D44** (1991) 1298.
- [11] E. Braaten and R.D. Pisarski, Phys. Rev. Lett. **64** (1990) 1338; Phys. Rev. **D42** (1990) 2156; Nucl. Phys. **B337** (1990) 569.
- [12] R.D. Pisarski, Phys. Rev. Lett. **63** (1989) 1129.
- [13] V.V. Lebedev and A.V. Smilga, Phys. Lett. **B253** (1991) 231; Ann. Phys. **202** (1990) 229; Physica **A181** (1992) 187.

- [14] R.D. Pisarski, Phys. Rev. **D47** (1993) 5589.
- [15] J.-P. Blaizot and E. Iancu, Phys. Rev. Lett. **76** (1996) 3080; Phys. Rev. **D55** (1997) 973.
- [16] M.H. Thoma, Z. Phys. **C66** (1995) 491.
- [17] B. Vanderheyden and J.-Y. Ollitrault, in preparation.
- [18] E. Braaten and T.C. Yuan, Phys. Rev. Lett. **66** (1991) 2183.
- [19] J.M. Luttinger, Phys. Rev. **121** (1961) 942.
- [20] T. Holstein, R.E. Norton and P. Pincus, Phys. Rev. **B8** (1973) 2649.
- [21] J.-P. Blaizot and E. Iancu, Nucl. Phys. **B390** (1993) 589; Phys. Rev. Lett. **70** (1993) 3376.
- [22] M.H. Thoma, Phys. Rev. **D51** (1995) 862.
- [23] M. le Bellac and C. Manuel, Phys. Rev. **D55** (1997) 3215.
- [24] R.D. Pisarski, Physica A **158** (1989) 146.
- [25] V.P. Silin, Sov. Phys. JETP **11** (1960), 1136.
- [26] H.A. Weldon, Phys. Rev. **D26** (1982) 1394.
- [27] V.V. Klimov, Sov. J. Nucl. Phys. **33** (1981) 934.
- [28] H.A. Weldon, Phys. Rev. **D26** (1982) 2789.
- [29] H.A. Weldon, Phys. Rev. **D28** (1983) 2007.
- [30] L. Kadanoff and G. Baym, “Quantum Statistical Mechanics,” W.A. Benjamin, New-York, 1962; R.L. Kobes and G.W. Semenoff, Nucl. Phys. **B260** (1985) 714; Nucl. Phys. **272** (1986) 329; M. le Bellac, *Thermal field theory*, Cambridge University Press, Cambridge, 1996.

FIGURE CAPTIONS

Figure 1: Left: Tree diagram for e^-e^- scattering. Right: Two-loop self-energy diagram. The imaginary part, obtained by cutting the diagram through the fermion loop, corresponds to the amplitude on the left, squared and integrated over phase space.

Figure 2: Left: Diagram for e^-e^- scattering with a screened interaction. The resummed photon propagator is indicated by a blob. Middle: One-loop self-energy diagram with a resummed photon propagator. Right: Emission of a virtual soft photon by a hard electron, corresponding to small angle e^-e^- scattering.

Figure 3: Tree diagrams for Møller scattering.

Figure 4: Two-loop self-energy diagrams corresponding to the scattering processes depicted in Fig. 3. The diagram on the left gives the direct and exchange contribution while the diagram on the right is the interference term.

Figure 5: Tree diagrams for (a) Bhabha scattering and (b) pair annihilation.

Figure 6: left: Tree diagram for e^+e^- annihilation. As in Fig. 2 (left), the exchange diagram is negligible when the momentum carried by the internal propagator is soft. Right: Emission of a soft virtual positron (or absorption of a soft electron) by a hard positron, representing the contribution of soft momentum transfers to the process on the left.

Figure 7: Self-energy diagrams corresponding to positron scattering and annihilation. The three two-loop diagrams correspond to the hard contribution: the first diagram corresponds to direct and exchange terms in Bhabha scattering (Fig. 5a), the second to direct and exchange terms in pair annihilation (Fig. 5b), while the third diagram, which can be cut in two different ways, gives the interference terms of both processes; finally, the one-loop diagram on the

right corresponds to the soft contribution to pair annihilation.

Figure 8: Tree diagrams for electromagnetic and Yukawa Compton scattering.

Figure 9: Left: Leading diagram for Compton scattering in the limit of soft exchanged momenta. Right: Emission of a soft virtual positron (or absorption of a soft electron) by a hard photon, corresponding to the process on the left.

Figure 10: Self-energy diagrams corresponding to Compton scattering. The three two-loop diagrams correspond to the hard contribution: the first and second diagrams correspond respectively to the first and second processes in Fig. 8, while the third diagram is the interference term; finally, the one-loop diagram on the right corresponds to the soft contribution.

Figure 11: Tree diagrams of gluon Compton scattering. The first of the three diagrams dominates when the momentum carried by the internal gluon is soft.

Figure 12: Emission of a soft virtual gluon by a hard gluon, representing the contribution of soft momentum transfers to the process depicted in Fig. 11.

Figure 13: One-loop self-energy diagram contributing to the gluon damping rate through Compton scattering at small angles.

Figure 14: Damping rate of hard one-particle excitations in the Yukawa theory as a function of their momentum p . We have chosen for e the numerical value $e^2/4\pi = 1/137$. Full line: fermion ($p > \mu$, eq. (12)) and hole ($p < \mu$, eq. (14)) excitations; long dashes: antifermion

(eqs. (17) and (28)); short dashes: boson (eq. (44)).

Figure 15: Same as Figure 14 for QED interaction.

Figure 16: Same as Figure 14 for QCD interaction, with $N_f = 2$ flavors. The numerical value of the coupling constant is the same as in Figs. 14 and 15.

Figure 17: One loop resummed diagram contributing to the electron or quark damping rate.

$$\sum_{k,q} \left| \begin{array}{ccc} k & \longrightarrow & k' \\ & \text{wavy } q, \omega & \\ p & \longrightarrow & p' \end{array} \right|^2 = -2 \text{Im} \left[\begin{array}{c} \text{triangle with loop} \\ \longrightarrow \end{array} \right]$$

Figure 1

$$\sum_{k,q} \left| \begin{array}{ccc} k & \longrightarrow & k' \\ & \text{wavy } q, \omega \text{ with dot} & \\ p & \longrightarrow & p' \end{array} \right|^2 = -2 \text{Im} \left[\begin{array}{c} \text{triangle with dot} \\ \longrightarrow \end{array} \right] = \sum_q \left| \begin{array}{ccc} & & q, \omega \\ & \text{wavy } q, \omega \text{ with dot} & \\ p & \longrightarrow & p' \end{array} \right|^2$$

Figure 2

$$\begin{array}{ccc} k & \longrightarrow & k' \\ & \text{wavy } q, \omega & \\ p & \longrightarrow & p' \end{array} - \begin{array}{ccc} k & \longrightarrow & k' \\ & \text{wavy } q, \omega & \\ p & \longrightarrow & p' \end{array}$$

Figure 3

$$\begin{array}{c} \text{triangle with loop} \\ \longrightarrow \end{array} + \begin{array}{c} \text{triangle with loop} \\ \longrightarrow \end{array}$$

Figure 4

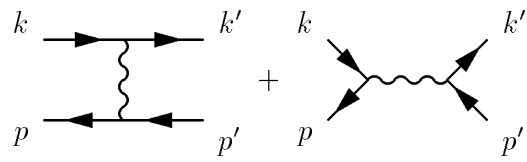


Figure 5 a

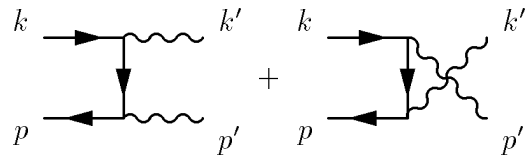


Figure 5 b

$$\sum_k \left| \begin{array}{c} k \rightarrow \text{---} \text{---} \text{---} k' \\ | \\ \bullet \text{---} q, \omega \\ | \\ p \leftarrow \text{---} \text{---} \text{---} p' \end{array} \right|^2 = \left| \begin{array}{c} \text{---} \text{---} \text{---} q, \omega \\ | \\ \bullet \\ | \\ p \leftarrow \text{---} \text{---} \text{---} p' \end{array} \right|^2$$

Figure 6

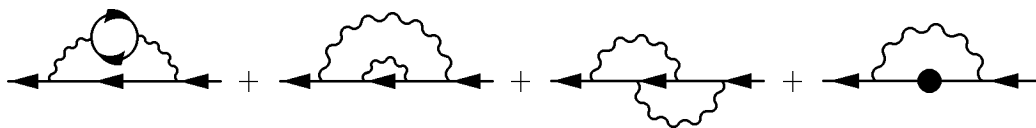


Figure 7

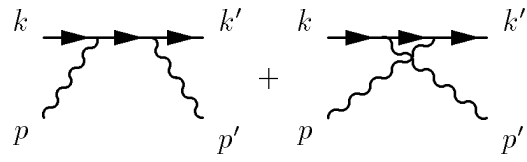


Figure 8

$$\sum_k \left| \begin{array}{c} k \xrightarrow{q, \omega} k' \\ \text{wavy line } p \text{ to } p' \end{array} \right|^2 = \left| \begin{array}{c} \text{wavy line } p \text{ to } k' \\ \text{fermion } k \text{ to } k' \end{array} \right|^2$$

Figure 9

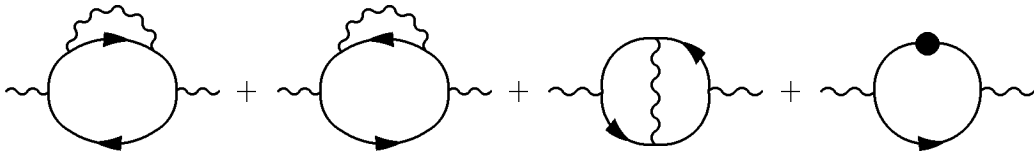


Figure 10

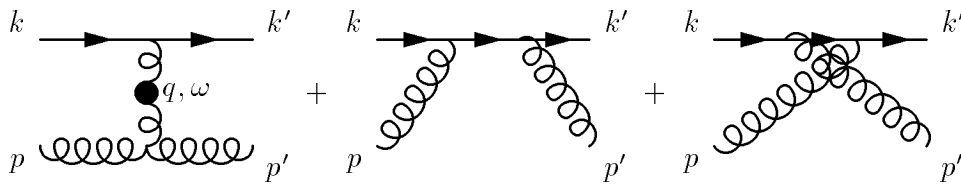


Figure 11

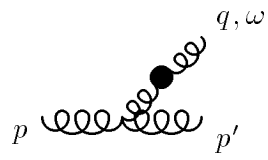


Figure 12

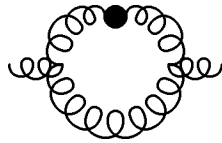


Figure 13

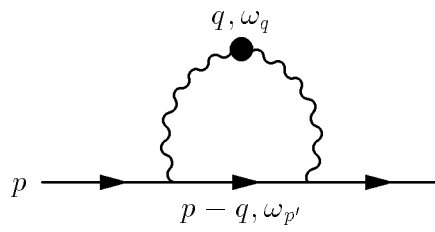


Figure 17

Figure 14

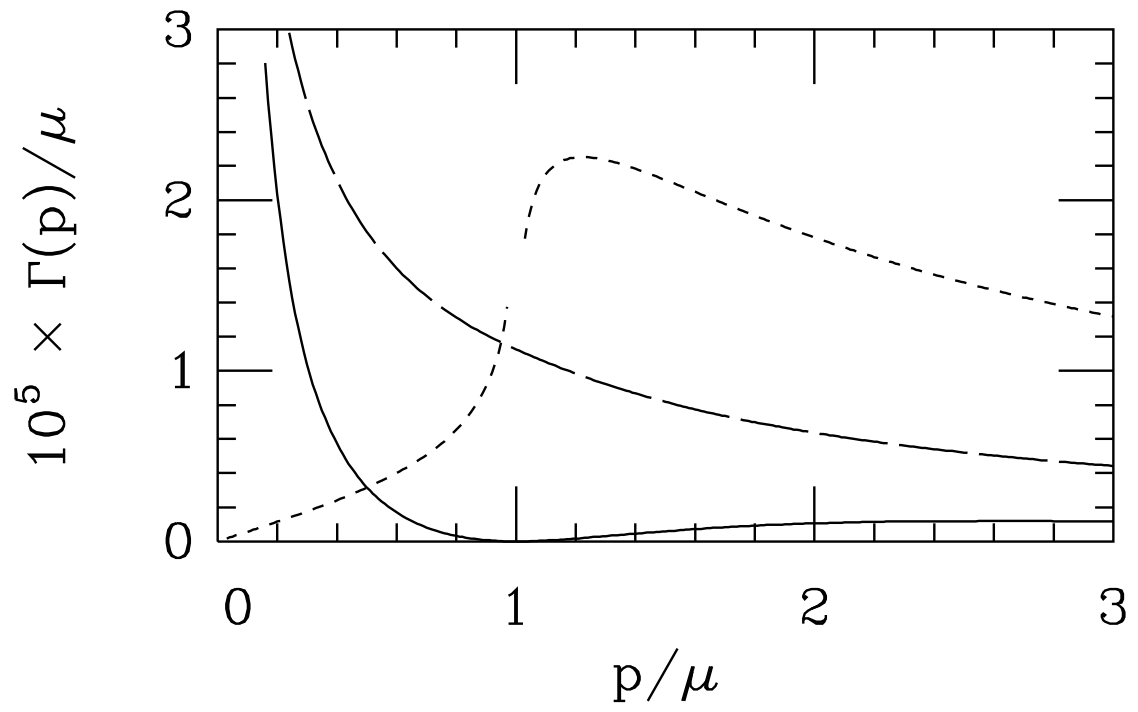


Figure 15

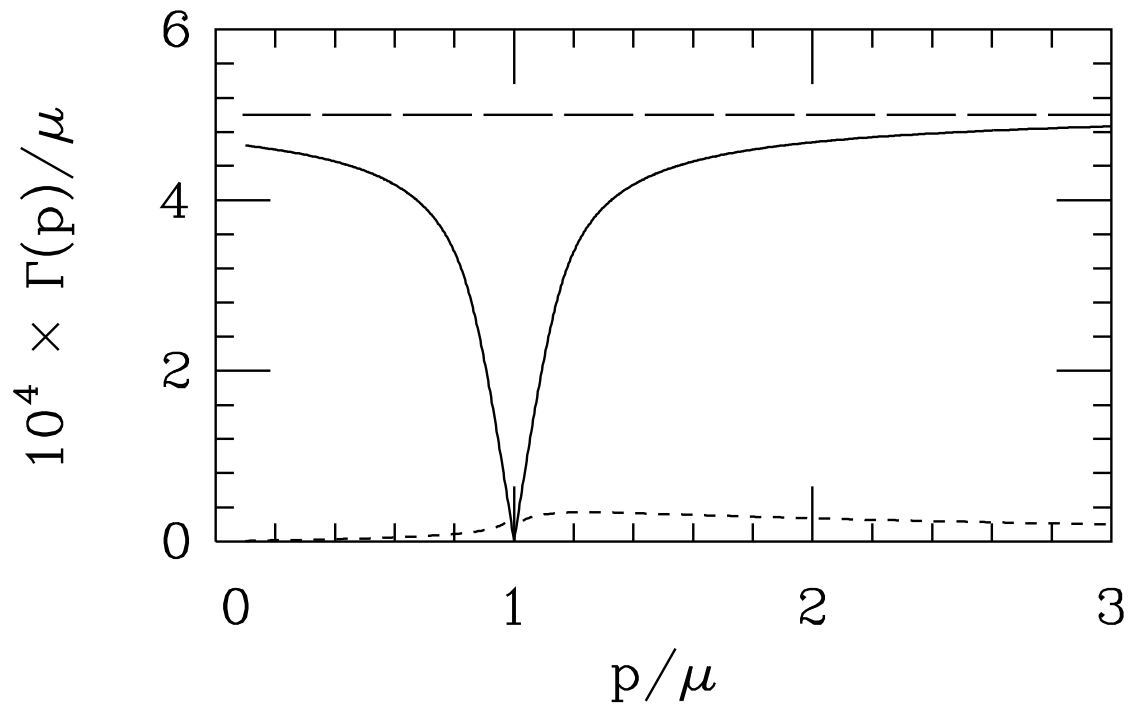


Figure 16

